Aerosol Science and Technology
Publication details, including instructions for authors and subscription information:
http://www.tandfonline.com/loi/uast20

A Multidomain Magnetic Passive Aerosol Sampler: Development and Experimental Evaluation

Ta-Chih Hsiao [a b], Peter A. Jaques [c] & Pengfei Gao [a]

[a] National Institute for Occupational Safety and Health, National Personal Protective Technology Laboratory, Pittsburgh, Pennsylvania, USA

[b] Graduate Institute of Environmental Engineering, National Central University, Jhongli City, Taoyuan County, Taiwan

[c] URS Corporation, Pittsburgh, Pennsylvania, USA

Accepted author version posted online: 27 Aug 2012.Version of record first published: 14 Sep 2012.

To cite this article: Ta-Chih Hsiao, Peter A. Jaques & Pengfei Gao (2013): A Multidomain Magnetic Passive Aerosol Sampler: Development and Experimental Evaluation, Aerosol Science and Technology, 47:1, 37-45

To link to this article: http://dx.doi.org/10.1080/02786826.2012.724186

Aerosol Science and Technology, 47:37–45, 2013
ISSN: 0278-6826 print / 1521-7388 online
DOI: 10.1080/02786826.2012.724186

A Multidomain Magnetic Passive Aerosol Sampler: Development and Experimental Evaluation

Ta-Chih Hsiao,[1,2] Peter A. Jaques,[3] and Pengfei Gao[1]

[1]*National Institute for Occupational Safety and Health, National Personal Protective Technology Laboratory, Pittsburgh, Pennsylvania, USA*
[2]*Graduate Institute of Environmental Engineering, National Central University, Jhongli City, Taoyuan County, Taiwan*
[3]*URS Corporation, Pittsburgh, Pennsylvania, USA*

An innovative "quarter-sized" multidomain magnetic passive aerosol sampler (MPAS) has been developed, mainly for determining particle penetration through personal protective ensembles. The MPAS is a 28 mm disc with a height of 8.6 mm. It consists of 186 small magnets with about 140 on the collection area, arranged in an alternating N and S pole pattern. In contrast to conventional passive samplers, it uses magnetic force to collect a quantifiable amount of surrogate Fe_3O_4 particles within a substantially shortened sampling time. This article presents detailed design, principles of operation, performance evaluation, and the development of a deposition velocity model for the MPAS. Performance of the MPAS was evaluated under various test conditions, including different particle sizes ranging from 95 to 350 nm and wind speeds ranging from 0.48 to 1.17 m/s. A previously developed recirculation aerosol wind tunnel was employed to evaluate its performance. Experimental results show that the dimensionless deposition velocity increased with increasing particle size (e.g., about 5-fold greater for 300 nm particles than 100 nm particles at 0.48 m/s) and slightly decreased with increasing wind speeds. Our results show that this sampler is promising for the measurement of particle penetration through protective ensembles for which high collection efficiency is needed.

[Supplementary materials are available for this article. Go to the publisher's online edition of *Aerosol Science and Technology* to view the free supplementary files.]

1. INTRODUCTION

Exposure to aerosol may pose a risk to adverse health effects (Behrens et al. 2002; Kirchner et al. 2005). Protective ensembles are used as barriers against dermal exposures to particulate hazards, including nanoparticles in the workplace (Hersh and Tucker 1993). In order to determine how well ensembles protect wearers, it is necessary to test the entire suit system while being worn to measure potential leakage through seams, closures, areas of transition to other protective equipment, and any leakage due to movement and activities. However, current test methods for particle penetration through protective ensembles are mainly based on active filtration principles, which deviate from "real world" experiences. Actually, particle penetration through protective ensembles is primarily driven by upstream wind rather than a downstream vacuum (Gao et al. 2011). Thus, a test method that does not depend on filtration-based approaches is important to more accurately evaluate particle penetration. Furthermore, a system-level aerosol test (i.e., aerosol man-in-simulant test [MIST]) that uses a passive sampler, similar to the chemical MIST (ASTM 2012) utilizing passive adsorbent dosimeters ($25 \times 35 \times 2$ mm), is currently lacking. A total of 30 dosimeters need to be placed at different locations under the protective clothing layer by a human subject who performs a series of physical exercises for a short time period of 30 min (ASTM 2012). The dosimeter must be small, light, pump-free, and have relatively high collection efficiency.

Although several existing passive aerosol samplers are unique for various applications, they are not suitable for the

Received 5 June 2012; accepted 11 August 2012.

The authors are thankful to Drs. William King at NIOSH and Zhong-Min Wang currently with the California Department of Public Health for their help on developing the previous prototypes of the sampler and conducting some preliminary experiments; Dr. Lin Li of Department of Mechanical Engineering, University of Minnesota for characterizing the magnetic susceptibility of aerosolized Fe_3O_4 particles; Christiana Lee, a summer student from the University of Florida for conducting some experiments; Dr. Philip K. Hopke of Clarkson University, Dr. Benjamin C. Eimer at URS Corporation, and Dr. Seung Won Kim at NIOSH for their review of the manuscript and valuable comments and suggestions. Part of this research was performed while Dr. Ta-Chih Hsiao held National Research Council Resident Research Associateship at NIOSH. The findings and conclusions of this report are those of the authors and do not necessarily represent the views of the National Institute for Occupational Safety and Health.

Address correspondence to Pengfei Gao, National Institute for Occupational Safety and Health, National Personal Protective Technology Laboratory, 626 Cochrans Mill Road, Pittsburgh, PA 15236, USA. E-mail: PGao@cdc.gov

aerosol MIST procedure, because they either have low collection efficiency that results in unacceptably long testing times, or an inadequate physical sampler size and/or targeted particle size range. For instance, Brown et al. (1994a, 1994b) developed a passive aerosol sampler using a permanently charged polymer sheet (an electret) as the sampling substrate. Particle deposition rate was independent of air velocity when the velocity exceeded the critical value. Although the sampler was small, lightweight, and pump-free, the collection efficiency was not high enough for an aerosol MIST, requiring greater than 5 h. Additionally, under high humidity conditions (e.g., sweat during MIST activities), the charge of the particles and electret could be significantly affected. Vinzents (1996) proposed a passive aerosol sampler, larger and heavier than the one developed by Brown et al., using three transparent sticky foils facing upward, forward, and downward as sampling substrates. A light extinction technique was deployed to measure the amount of collected dust, and a pure empirical model was created to estimate dust concentrations. Wagner and Leith (2001) developed a miniature passive aerosol sampler and established a semiempirical deposition velocity model for determining average particle concentration and size distribution in the air. They used scanning electron microscopy (SEM) to analyze the collected particles. Thus, in addition to particle number, the information of particle size and morphology was provided. Their experimental results show that the ambient deposition velocity is largely independent of the turbulent friction velocity for particle sizes larger than 0.5 μm under most indoor and outdoor wind conditions. However, to collect a statistically significant number of particles, the Wagner and Leith sampler generally requires sampling between several days to more than a week, which is out of the time scale of the aerosol MIST. Recently, a personal aeroallergen sampler (PAAS) was proposed by Yamamoto et al. (2006). It collects particles by gravitational settling and has a special design to enable the collection surface to be consistently directed upward regardless of inclination of the sampler. However, the sampler requires a long sampling time, and is mainly used for coarse particle sampling.

Therefore, a magnetic passive aerosol sampler (MPAS) was developed for possible use in the aerosol MIST, and for determining particle penetration through test swatches of protective clothing materials. Iron (II, III) oxide (i.e., Fe_3O_4) particles were used as the surrogate agent. This article presents the design and principles of operation, development of a deposition velocity model, and the performance evaluation of the MPAS under various test conditions.

2. DESIGN OF THE MPAS

As shown in Figure 1, the multidomain MPAS consists of a 28 mm diameter aluminum body with a thickness of 8.6 mm. A total of 186 miniature square magnets (1.5 × 1.5 × 0.75 mm, Gaussboys Super Magnets, Portland, OR, USA) are arranged with an alternating N and S pole pattern. The magnets are composed of neodymium, iron, and a trace amount of boron

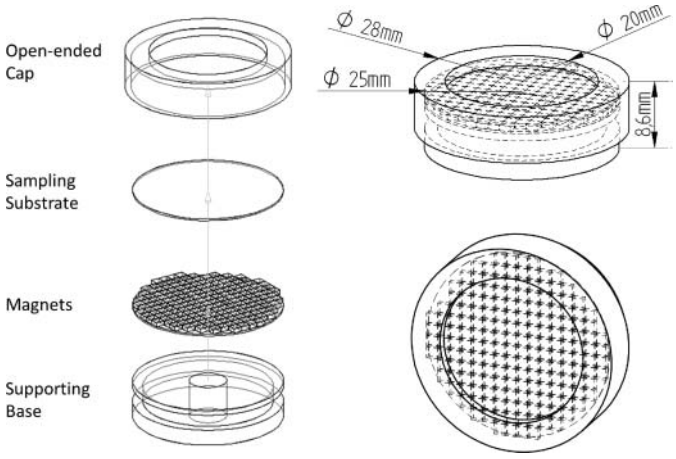

FIG. 1. Schematic diagram of the multidomain MPAS.

(Nd2 Fe14 B, grade N38). They are also coated with nickel (10–20 microns thick) to protect against corrosion. An open-ended circular cap is used to secure the magnets and a sampling substrate is seated directly on the top of the magnets. The cap also maintains a distance of 1.5 mm between the sampler opening and the magnet surface to separate the magnets from the test fabric. The collection region (20 mm in diameter), which contains about 140 magnets, is confined by the cap. The remaining 46 magnets are covered by the cap and are outside the collection region. A 25 mm polycarbonate substrate is used to collect particles.

In the early stages of this study, a single-domain MPAS was also fabricated and compared to the multidomain MPAS. It contains only one comparatively large magnet with a diameter of 18 mm and a thickness of 3 mm (NdFeB grade N35, nickel-plated; Gaussboys Super Magnets, Portland, OR, USA). The peak magnetic field strength is about the same as that for the multidomain unit.

In order to take advantage of the enhanced collection potential from its magnetic field, the MPAS needs to be operated with particles of paramagnetic material, such as iron oxide. In this study, magnetite (Fe_3O_4) stock powder (Alfa Aesar 12962, Puratronic®, 99.997%, Ward Hill, MA, USA) was used because of the greatest magnetic susceptibility it has among iron oxide particles. In addition, iron oxide is relatively low in toxicity with an OSHA PEL of 10 mg/m^3.

3. DEPOSITION VELOCITY MODEL

Particles collected by passive aerosol samplers are generally controlled by turbulent diffusion, Brownian diffusion, gravitational settling, inertial impaction, and thermophoretic drift combined with attraction due to electric forces or, in the case of this study, magnetic force. Several models have been reported for predicting the particle deposition rate or the particle flux onto various surfaces, such as human skin (Scheneider et al. 1994), walls of residential buildings (Lai 2005; Zhao et al.

2010), semiconductor wafers (Liu and Ahn 1987; Cooper et al. 1989; Turner et al. 1989), works of art in museums (Nazaroff et al. 1990a,b), and different plant leafs (Slinn 1982). By considering some of these theoretical deposition models, along with an evaluation of particle deposition in still air conditions, Cheng (1997) summarized that slight changes in temperature result in deposition by convective eddy diffusion ("natural convection"), and that natural convection causes turbulent mixing, independent of forced mixing, resulting in diffusional deposition predominantly for particles less than 0.1 μm, while deposition by sedimentation is dominant for particles greater than 1.0 μm. For a conventional passive aerosol sampler, there is generally an absence of electrical charging and a negligible temperature gradient on the surface, while turbulent diffusion and Brownian diffusion are considered the primary capture mechanisms for particle size less than 100 nm. As particle size increases, gravitational setting and inertial impaction would become dominant over diffusion and play an important role on the deposition rate. In most studies, the deposition rate is characterized by the deposition velocity (V_{dep}), which has the dimension of velocity, and is defined as the ratio of the particle flux (particle transport to the collecting surface per unit area per time, J_{dep}) to the reference concentration in the bulk flow (C_∞), i.e.,

$$V_{\text{dep}} = J_{\text{dep}}/\text{C}_\infty. \quad [1]$$

For passive aerosol samplers, the particle deposition flux, J_{dep}, can be calculated based on the mass or number of particles collected on the surface, since the sampling time and sampling area are known. Therefore, in order to convert the amounts passively collected to particle concentration in the air (C_∞), estimation of the deposition velocity (V_{dep}) is essential. Note that the deposition velocity sometimes is referred as the mass transfer coefficient (K_m), especially for those models using the mass transfer correlation between Sherwood number ($\text{Sh} = K_m \cdot l/D_p$), Schmidt number ($\text{Sc} = \nu_g/D_p$), and Reynolds number ($\text{Re} = lV_\infty/\nu_g$), or Peclet number ($\text{Pe} = lV_\infty/D_p$) in analogy to fluid heat and mass transfer. Here, ν_g is the kinematic viscosity of air, l is the characteristic length, V_∞ is the bulk flow velocity, and D_p is the Brownian diffusivity of the particle.

To evaluate the deposition velocity theoretically, the convective diffusion equation is usually solved near the collecting surface along with following assumptions:

1) The fluid is incompressible and the particles are intertialess;
2) The particle deposition flux (J_{dep}) is one-dimensional and steady;
3) The particle transportation through concentration boundary layer is described by Brownian and turbulent diffusion together with other driving forces, i.e., the concentration boundary layer thickness, δ_c, equals to the diffusion boundary layer thickness, δ_D;
4) The concentration boundary layer thickness, δ_c, is much smaller than the momentum boundary layer (δ_m), i.e., the fluid axial velocity is negligible within the concentration boundary layer.

However, assumptions (3) and (4) may not be valid for the case in this study, which will be discussed with the resultant model.

The dimensionless particle deposition velocity ($\tilde{V}_{\text{dep}} = V_{\text{dep}}/V_\infty$) can then be expressed as

$$\tilde{V}_{\text{dep}} = -\left(\frac{D_{Ep} + D_p}{\nu_g}\right)\frac{d\tilde{C}}{d\tilde{z}} + \tilde{V}_{\text{ext}}\tilde{C}, \quad \text{and} \quad \tilde{z} = \frac{zV_\infty}{\nu_g}, \quad [2]$$

where the variables are defined in the Nomenclature section.

The dimensionless deposition velocity for the MPAS, $\tilde{V}_{\text{dep}}$, can then be expressed as Equation (3)

$$\tilde{V}_{\text{dep}} = \tilde{V}_{\text{mag,avg}}\left(1 - \frac{1.375\alpha l\text{Re}^{-0.5}}{z_0}\right) \pm \tilde{V}_T, \quad [3]$$

where

$$\tilde{V}_{\text{mag,avg}} = \frac{32}{3}\frac{C_c}{C_D\text{Re}_p\eta}\cdot\frac{R_p^2\Delta\chi\mu_0}{V_\infty}\cdot\frac{\int_{A_M} H_{\max}(x,y)\frac{dH}{dz}dxdy}{\int_{A_M} dxdy},$$

and $$\tilde{V}_T = \frac{16}{3}\frac{C_c}{C_D\text{Re}_p\eta}\cdot\frac{R_p^2\rho_P g}{V_\infty},$$

where α is an empirical coefficient representing a ratio of the thickness of the concentration boundary layer (δ_c) to the thickness of the momentum boundary layer (δ_m), i.e., $\alpha = \delta_c/\delta_m$. All the variables are defined in the Nomenclature section. Detail derivations of the deposition velocity model are presented in Section A of the online supplemental information.

4. EXPERIMENTAL

4.1. Characterization of the Magnetic Field for the MPAS

The magnetic field generated by the multidomain MPAS was measured with a gauss meter housed with an active tip area of 0.127 mm^2 (Model 6010, Sypris Test & Measurement, Inc., Orlando, FL, USA). A compact dovetail linear stage laser stand (Model DS40-XYZ, Newport Corp., CA, USA) was used to orient the sensor along the x–y plane and away from the surface along the z-axes. The field strength of the 2 × 2 section (a block of four magnets) was scanned at 0.1 mm increments across the surface and up to 1.253 mm away from the surface.

4.2. Performance Evaluation Using a Recirculation Aerosol Wind Tunnel (RAWT)

4.2.1. Aerosol Generation

A RAWT was employed for the performance evaluation of the MPAS (Figure 2). Fe_3O_4 stock powder was mixed in

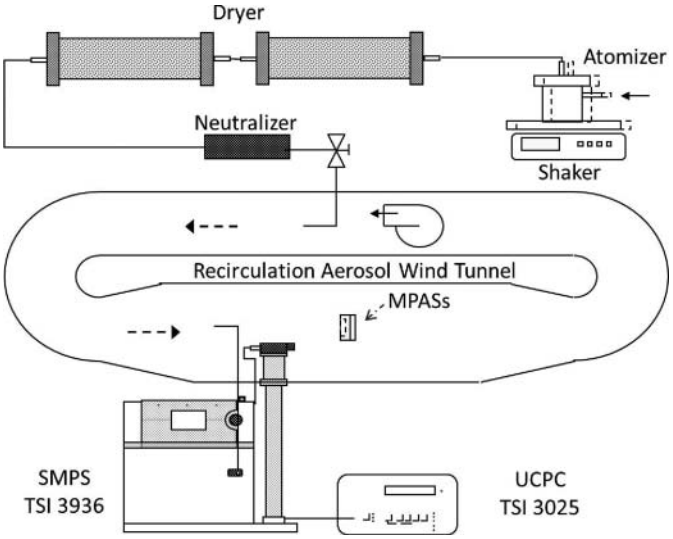

FIG. 2. Schematic diagram of experimental setups for the performance evaluation of the MPAS.

deionized water and aerosolized with a prototype Collison atomizer to generate the challenge aerosol. Before atomization, the suspension was sonicated for 5 min to break up the agglomerated stock powder. An atomizer was seated on a rotational shaker (Innova 2300, New Brunswick Scientific, Edison, NJ, USA) to agitate and keep the Fe_3O_4 particles uniformly distributed in suspension during the atomizing process and to ensure a stable aerosol concentration and size distribution in the RAWT during the performance evaluation. The generated mist was passed through a series of diffusion dryers to produce dry Fe_3O_4 particles, and to reduce particle losses passed through an aerosol charge neutralizer (TSI 3012). Due to the recirculation design of the RAWT, wind velocity was easily adjusted with its integrated blower, but without adding or removing dilution air. This allowed the system to reach a steady challenge aerosol concentration for the MPAS evaluation for different wind velocities. Previously, a spatially uniform air flow and aerosol concentration was found in the RAWT with a coefficient of variation less than 9% for all wind conditions and particle sizes (Jaques et al. 2011). The size distribution of aerosol in the RAWT evaluation had an average count mean diameter of 135 nm with peak concentrations of 10^5 #/cm^3.

4.2.2. *Characterization of the Magnetic Susceptibility of Fe_3O_4 Particles*

Magnetic susceptibility of Fe_3O_4 particles is an important parameter in developing a deposition velocity model for the MPAS. Magnetic susceptibility is a dimensionless proportionality constant that indicates the degree of magnetization of a material in response to an applied magnetic field. To characterize the magnetic susceptibility of aerosolized Fe_3O_4 particles, a magnetic filter (Li et al. 2011) was used. The magnetic filter consists of a set of parallel 200 mesh screens made of stainless steel magnetic wires (SS 430). The carrier gas loaded with magnetic particles flowed through the filter element in the direction perpendicular to the screens. The mesh screens are magnetized by an external magnetic field in the axial direction produced by an electrical coil surrounding the circumference of the cell. The subsequent deposition or trapping of particles in the magnetic screen set is governed by the magnetic force that particles experience in the neighborhood of the magnetized screen wires.

Fe_3O_4 aerosol was generated for the magnetic susceptibility measurements. To quantify particles by size, a differential mobility analyzer (DMA; TSI Model 3081, TSI Incorporated, Shoreview, MN, USA) was placed downstream from the aerosol generation system to classify singly charged, monodisperse particles in the size range from 95 to 350 nm. Prior to being introduced into the DMA, the polydisperse stream was passed through a Kr^{85} radioactive particle charger to impart a well-defined charge distribution. For particles with diameters ranging from 95 to 300 nm, the DMA was operated at an aerosol flow rate of 1.5 lpm with a sheath flow rate of 15.0 lpm, and for particles larger than 300 nm, the sheath flow was adjusted to 8.0 lpm, while maintaining the same aerosol flow rate. Since the classified particles that passed through the DMA were electrically charged, a Po^{210} neutralizer and an electrostatic condenser were used downstream to obtain electrically neutral test particles of the desired size. Particle number concentrations both upstream and downstream of the magnetic filter system were measured by an ultrafine condensation particle counter (UCPC, TSI Model 3025, TSI Incorporated, Shoreview, MN, USA). Particle penetration through the magnetic filter was derived as a ratio of concentration upstream to concentration downstream. Since penetration through the magnetic filter is a function of particle size, magnetic susceptibility, magnetic field, and flow field, magnetic susceptibility was then calculated from the measured penetration data using a particle trajectory model as described by Li et al. (2011). For instance, for a given particle size at defined magnetic field and flow field, particle penetration was calculated assuming a series of susceptibilities from which penetration as a function of particle susceptibility was plotted. Based on the curve, corresponding susceptibilities were interpolated using the penetration data.

4.2.3. *Experimental Determination of Deposition Velocity of the MPAS*

The deposition velocity (V_{dep}), defined as the ratio of the particle flux (particle transport to the collecting surface per unit area per time, J_{dep}) to the reference concentration (C_∞), is the primary parameter for evaluating the MPAS performance. However, for monodisperse submicron particles, including those that are in the nanosize range, the amount collected on the MPAS substrate was near the limits of detection for wet chemical or mass-balance methods. Thus, inspired by the work done by Okuyama et al. (1986) in estimating the particle deposition rate coefficient (β) using V_{dep} and the area of the collection surface, we evaluated V_{dep} of particles onto the MPAS according

to Equation (4) by measuring and comparing values of β of the RAWT and the MPASs with and without magnets. Detailed derivation of the equation is presented in Section B of the online supplemental information.

$$V_{\text{dep}}(d_p) = \left[\frac{\exp(-\beta_{wo}(d_p)\cdot\tau) - \exp(-\beta_w(d_p)\cdot\tau)}{1-\exp(-\beta_w(d_p)\cdot\tau)}\right] \times \frac{V_{WT}\cdot\beta_w(d_p)}{A_M}. \quad [4]$$

The values of β for the RAWT, the RAWT including MPASs with magnets (β_w), and the RAWT including the MPASs without magnets (β_{wo}) were determined by calculating the decay rate of the particle number concentration. For each test, a total of 12 MPASs were placed evenly across a cross-section of the RAWT test section. Once a constant aerosol concentration was established, the atomizer was stopped, and the aerosol injection inlet and bypass port of the RAWT were capped to insure a closed system. A scanning mobility particle sizer (SMPS, TSI Model 3936, TSI Incorporated, Shoreview, MN, USA) was employed to measure particle size distribution inside the RAWT every 5 min over a time period of about 2 h.

In this study, the MPAS was examined facing vertically into the wind. Based on a survey done by Baldwin and Maynard (1998), background wind speeds in the workplace may be represented by a distribution with a mean value between 0.3 and 0.4 m/s. Therefore, to investigate the effect of wind velocity, experiments were conducted at three different wind velocities: 0.48, 0.78, and 1.17 m/s. In addition, for each experimental condition, the test was performed at least three times to enhance precision.

4.2.4. Determination of the Empirical Coefficient for the Deposition Velocity Model

For the practical MPAS application, linear regressions of the dimensionless deposition velocities, based on Equation (3) against those determined experimentally, were performed at a wind velocity of 50 cm/s by selecting different values of α until $y \approx x$ with a relatively high correlation is obtained.

5. RESULTS AND DISCUSSION

5.1. Magnetic Field of the MPAS and Particle Collection

Figure 3 shows that the magnetic field of each magnet of the multidomain MPAS is spatially symmetric with respect to its center and the magnetic field distribution between magnets is very similar. In their side-by-side square arrangement, they form a quadropolar magnetic field pattern, with its field strength being both affected by the polarity of each magnet and the interaction of adjacent magnets. At the corners, the attractive forces of oppositely poled adjacent magnets are neutralized by repelling forces between same-polled adjacent magnets, causing the respective fields to cancel each other out to form nulls at all corners of adjacent magnets. It is shown that the magnetic field strength is greatest (2.3 kilogauss) at the center across the magnet's surface ($z = 0$ mm) (Figure 3a), and quickly decays to about 0.1 kilogauss, only 4%, at $z = 1.253$ mm away from the surface (Figure 3d). It was further estimated that the magnetic field strength dropped off to less than 2% at the sampler opening (i.e., $z = 1.5$ mm from the magnet's surface), and, thus, is expected to disappear at the outside surface of protective ensembles used in a MIST procedure. This is an important feature, because oversampling by pulling particles from outside of the ensemble due to the gradient of the magnetic field would be minimized.

Figure 4 shows a comparison of Fe_3O_4 particles deposited on a conventional passive sampler without using magnets, the single-domain MPAS, and the multidomain MPAS (from left to right). The three samplers were exposed simultaneously to collect polydisperse Fe_3O_4 aerosol at $1.5 \times 10^5/\text{cm}^3$ for 102 min inside the RAWT. It is visually observed that the single-domain MPAS caused a nonuniform particle deposition pattern, typically ring-shaped, which would obstruct accurate SEM analysis. In contrast, the multidomain MPAS not only considerably improved collection efficiency, in comparison to the conventional passive sampler, but also produced a uniform distribution of particle clusters across the entire substrate, in comparison to the single-domain MPAS. Since each cluster was created by an individual magnet with the same magnetic field strength, particle counting and sizing strategy was able to be developed for accurate analysis (Jaques et al. 2012). The significantly enhanced sampling efficiency of the multidomain MPAS makes it possible for the necessarily shortened time frame required by the MIST procedure.

5.2. Magnetic Susceptibility of the Fe_3O_4 Particles

Effective volume magnetic susceptibility of Fe_3O_4 particles in the size range from 95 to 350 nm at the estimated 20 kA/m external magnetic field is shown in Figure 5. The error bar of the given magnetic susceptibility data was determined from that of the penetration data, taking into account the UCPC flow fluctuation.

Generally, the derived effective volume magnetic susceptibility of Fe_3O_4 particles is almost constant in the studied size range. A gradual increase of the magnetic susceptibility of studied particles with decreasing particle size is observed, especially for 95 nm particles. One reason for this increase is probably due to the transition trend of the magnetic domain from pseudo-single toward single domain with decreasing Fe_3O_4 particle size. The number of domains in a particle is a function of its size and shape. Generally, larger particles can accommodate multiple domains, while smaller grains can only accommodate single domain. Between them there is a significant middle group with only a few domains, named pseudo-single-domain (Dunlop and Özdemir 1997; Evans and Heller 2003). The magnetic susceptibility decreases with increasing particle size in single domain, reaches the minimum values in pseudo-single-domain, and slowly increases with increasing size in multiple domains (Hunt et al. 1995; Svoboda 2004). The single-domain size of

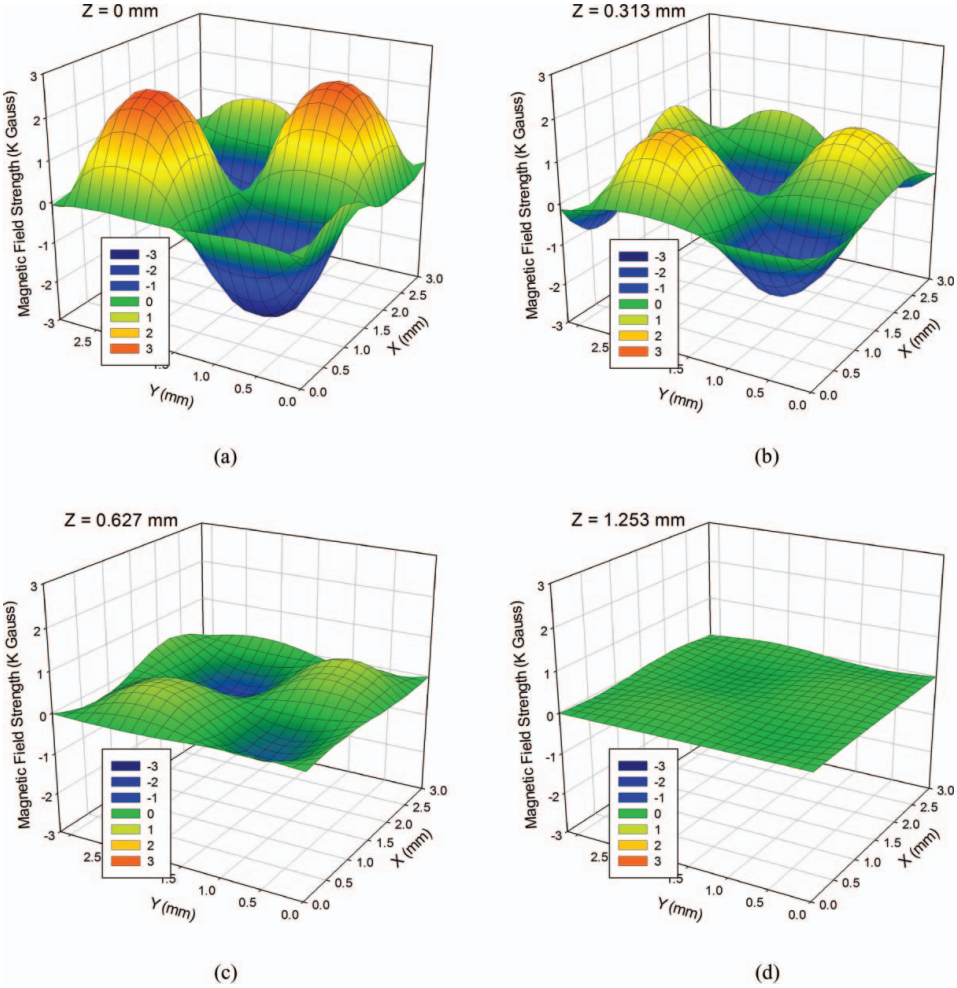

FIG. 3. Magnetic field of four adjacent magnets at different heights: (a) $z = 0$ mm, (b) $z = 0.313$ mm, (c) $z = 0.627$ mm, and (d) $z = 1.253$ mm.

magnetite is around 50 to 280 nm (Dunlop 1990). In this study, Fe_3O_4 particles start from pseudo-single-domain toward single domain with decreasing particle size. So the magnetic susceptibility is almost constant at larger particle sizes and increases at the smaller size particles. Another reason may be due to the classification of monodisperse particles. Some larger particles with multiple charges were selected and accounted for about 20% of tested monodisperse 100 nm particles from the initial bimodal size distribution. These reduced the penetration through the magnetic filter and overestimated the magnetic susceptibility of 100 nm Fe_3O_4 particles accordingly.

FIG. 4. Particle deposition patterns on a conventional passive sampler, a single-domain MPAS, and a multidomain MPAS (from left to right), which were exposed simultaneously inside the RAWT.

5.3. Experimental Determination of Deposition Velocities of the MPAS

5.3.1. Particle Deposition Rate Coefficients

In this study, the performance of the MPAS is mainly characterized in terms of the dimensionless deposition velocity ($\tilde{V}_{\text{dep}}$). Based on Equation (4), V_{dep} was determined by measuring the particle deposition rate coefficient of the RAWT and the MPASs with magnets (β_w) and the MPASs without magnets (β_{wo}). Figure 6 shows the ratios of particle number concentration to that at the initial time for the case of the RAWT and the MPASs with magnets and without magnets for two upstream wind velocities. In the log scale, the curves decreased linearly with elapsed time after the aerosol generation was stopped when a constant aerosol concentration was established, and the slope is the particle deposition rate coefficient, β. With the determined

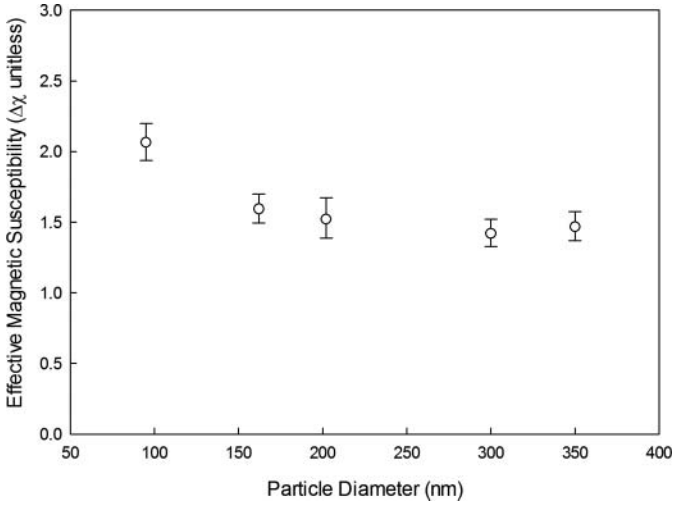

FIG. 5. Effective magnetic susceptibility of Fe_3O_4 particles that indicates the degree of magnetization of the particles in response to applied magnetic field. The error bars represent one standard deviation and $n = 3$.

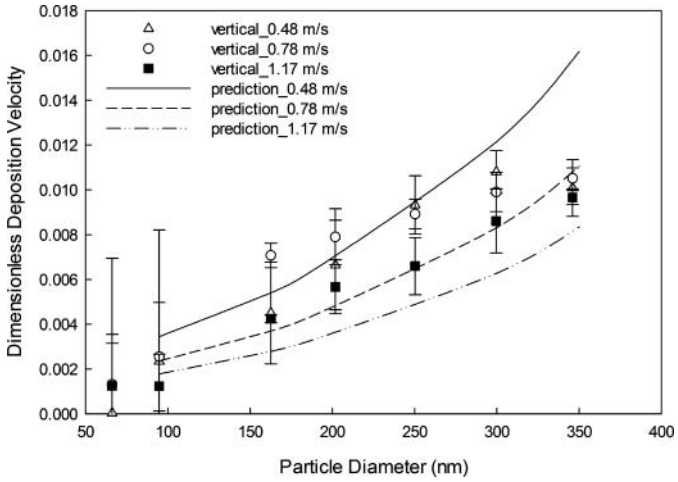

FIG. 7. Experimental and modeled dimensionless deposition velocity of the MPAS at three upstream wind velocities. The error bars represent one standard deviation and $n = 3$.

values of β at different wind velocities, V_{dep} can be determined as all the other variables in the equation are known.

Although the internal wall surfaces of the RAWT are much larger than the collection areas of the MPASs, the method was used to determine the rate coefficients because the decay rate of the RAWT without the samplers was constant over the elapsed time (Figure 6). In this study, a total of 12 MPASs were exposed simultaneously to increase the overall collection area of the samplers. Because of the magnetic force, particle loss per unit area on the MPASs was much larger than the MPAS without magnets.

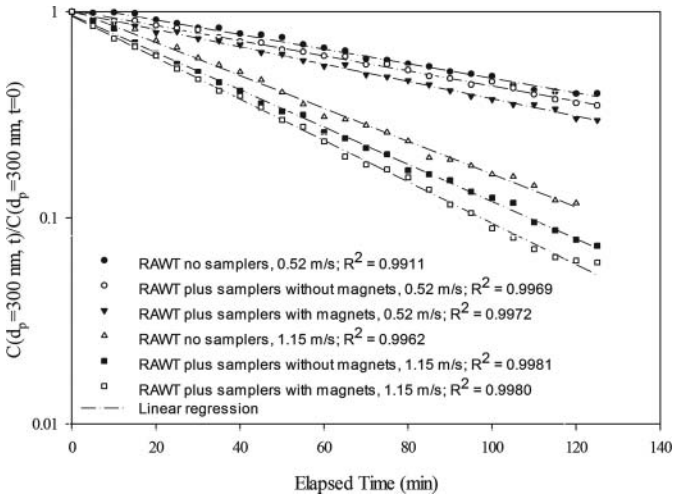

FIG. 6. Dimensionless particle concentration vs. elapsed time for the RAWT without MPAS, the RAWT plus MPASs with magnet, and the RAWT plus MPASs without magnet.

5.3.2. Dimensionless Deposition Velocities When Vertically Facing the Wind

The results of a series of measurements on $\tilde{V}_{dep}$ are plotted as a function of particle size for the MPAS when vertically facing the wind (Figure 7). $\tilde{V}_{dep}$increases with increasing particle size at all wind speeds tested. For example, $\tilde{V}_{dep}$ increased about 5-fold for particles from 100 to 300 nm at 0.48 m/s. A pairwise *t*-test between groups, using a Bonferroni correction, was performed to assess the difference between particles by size for different wind velocities. It is suggested that $\tilde{V}_{dep}$ may not be affected by wind velocity for all particle sizes ($p > 0.05$), except at 162.5 nm between 0.78 and 1.17 m/s. Therefore, the experimental data suggest that the velocity effect is relatively minor under the general range of indoor wind speeds. In addition, it can be observed that $\tilde{V}_{dep}$ is roughly linearly dependent on particle size.

According to the MPAS deposition velocity model (Equation (S11)), $\tilde{V}_{dep}$ is directly related to particle magnetic moment which is proportional to the cube of particle diameter and the effective volume magnetic susceptibility ($\Delta\chi$). Note, however, our magnetic filter measurements show that $\Delta\chi$ of the challenging Fe_3O_4 particles decreases gradually as particle diameter increases from 95 to 200 nm and then stays about the same level for larger particle sizes (Figure 5).

5.4. Deposition Velocity Model for the MPAS

For the practical MPAS application at a wind velocity of 50 cm/s, linear regressions of the calculated dimensionless deposition velocities based on Equation (3) against those determined experimentally were performed by selecting different values of α until $y \approx x$ was obtained. As a result, $y = x$ with a high correlation ($R^2 = 0.948$), resulted in $\alpha = 0.702$. Thus, the dimensionless deposition velocity,$\tilde{V}_{dep}$, is expressed as Equation

(5) for the MPAS

$$\tilde{V}_{\text{dep}} = \tilde{V}_{\text{mag,avg}}\left(1 - \frac{0.965l\text{Re}^{-0.5}}{z_0}\right) \pm \tilde{V}_T. \qquad [5]$$

Equation (5) indicates that δ_c is larger than δ_D, and δ_c is about 70% of the value of δ_m, thus assumption (3) addressed in Section 3 is not valid for the MPAS. Collection efficiency of the MPAS is significantly enhanced, as the transport in the concentration boundary layer is controlled by magnetic force instead of diffusion.

A comparison of the deposition velocities based on Equation (5) and the experimental determinations is also shown in Figure 7. It shows good agreement between the model predictions and the experimental measurements.

6. SUMMARY AND CONCLUSIONS

A small, thin, and light multidomain MPAS has been developed mainly for the aerosol MIST. The special design renders the following unique features: (1) magnetic force provides a much higher collection efficiency than a conventional passive sampler, which allows collecting a sufficient quantity of particles to fit within the time frame of a MIST procedure; (2) the multidomain arrangement allows magnetic force to disappear within a small distance between the sampler opening and the substrate to avoid overestimating penetration levels caused by pulling particles from the outside of ensembles; and (3) the multidomain arrangement also significantly improves uniformity of magnetite aerosol particle deposition across the substrate. In addition, the magnetic fields and forces generated by the permanent magnets are expected to be generally insensitive to environmental conditions, such as high relative humidity inside the ensemble due to sweat when the test subject performs a series of activities during a MIST procedure.

A deposition velocity model for the MPAS was developed that can be used to convert particle quantities passively collected by the sampler to air concentrations. Magnetic susceptibilities of the Fe_3O_4 particles at different sizes were measured in order for the development of the model. Performance of the MPAS was evaluated under various test conditions, including different particle sizes ranging from 95 to 350 nm and wind speeds ranging from 0.48 to 1.17 m/s. Experimental deposition velocity increased approximately linearly with increasing particle size, and the modeled $\tilde{V}_{\text{dep}}$was empirically fit to it. The results also show that the dimensionless deposition velocity slightly decreased with increasing wind speeds. However, the effect of wind velocity on dimensionless deposition velocity is minor under general indoor wind velocities or velocities that would be encountered inside a protective ensemble.

NOMENCLATURE

A_M	MPAS sampling area
C_c	Cunningham slip correction factor
C_∞	reference concentration
C_D	drag coefficient
$\tilde{C}$	dimensionless particle concentration ($\tilde{C} = C/C_\infty$)
D_{Ep}	eddy diffusivity of the particle
D_p	Brownian diffusivity of the particle
F_d	aerodynamic drag force on the particle
F_m	magnetic force
g	acceleration due to gravity
H	magnetic field
$H_{\max}(x,y)$	the maximum value of the magnetic field
J_{dep}	particle transport to the collecting surface per unit area per time
K_m	mass transfer coefficient
l	the characteristic length of the MPAS
m_m	particle magnetic moment
Pe	Peclet number ($\text{Pe} = lV_\infty/D_p$)
Re	Reynolds number ($\text{Re} = lV_\infty/\nu_g$)
R_p	particle radius
Sc	Schmidt number ($\text{Sc} = \nu_g/D_p$)
Sh	Sherwood number ($\text{Sh} = K_m \cdot l/D_p$)
u^*	the friction velocity
V_∞	bulk flow velocity
V_{dep}	deposition velocity
$\tilde{V}_{\text{dep}}$	dimensionless deposition velocity
$\tilde{V}_{\text{ext}}$	migration velocity due to the normal component of external forces normalized by bulk flow velocity V_∞
V_{mag}	magnetic drift velocity
$\tilde{V}_{\text{mag,max}}(x, y)$	maximum magnetic drift velocity
V_T	gravitational settling velocity
$\forall_{WT}$	total volume of the RAWT
α	empirical coefficient ($\alpha = \delta_c/\delta_m$)
β	particle deposition rate coefficient
β_w	particle deposition rate coefficient with the magnets (MPAS)
β_{wo}	particle deposition rate coefficient without magnets
μ_0	permeability of free space
δ_c	thickness of concentration boundary layer
δ_D	thickness of diffusion boundary layer
δ_m	thickness of momentum boundary layer
$\Delta\chi$	effective volume magnetic susceptibility of the particle relative to air
η	air viscosity
ν_g	kinematic viscosity of air
ρ_p	particle density
σ	particle stopping distance

REFERENCES

ASTM (American Society for Testing and Materials) (2012). *Standard Test Method for Man-IN-Simulant Test (MIST) for Protective Ensembles (Method F 2588-2012)*. American Society for Testing and Materials, Philadelphia, PA.

Baldwin, P. E. J., and Maynard, A. D. (1998). A Survey of Wind Speeds in Indoor Workplaces. *Ann. Occup. Hyg.*, 42(5):303–313.

Behrens, I., Vila Pena, A. I., Alonso, M. J., and Kissel, T. (2002). Comparative Uptake Studies of Bioadhesive and Non-Bioadhesive Nanoparticles in Human Intestinal Cell Lines and Rats: The Effect of Mucus on Particle Adsorption and Transport. *Pharm. Res.*, 19:1185–1193.

Brown, R. C., Wake, D., Thorpe, A., Hemingway, M. A., and Roff, M. W. (1994a). Theory and Measurement of the Capture of Charged Dust Particles by Electrets. *J. Aerosol. Sci.*, 25:149–163.

Brown, R. C., Wake, D., Thorpe, A., Hemingway, M. A., and Roff, M. W. (1994b). Preliminary Assessment of a Device for Passive Sampling of Airborne Particulate. *Ann. Occup. Hyg.*, 38:303–318.

Cheng, Y. S. (1997). Wall Deposition of Radon Progeny and Particles in a Spherical Chamber. *Aerosol Sci. Technol.*, 27:131–146.

Cooper, D. W., Peters, M. H., and Miller, R. J. (1989). Predicted Deposition of Submicrometer Particles Due to Diffusion and Electrostatics in Viscous Axisymmetric Stagnation-Point Flow. *Aerosol Sci. Technol.*, 11:133–143.

Dandy, D. S., and Yun, J. (1997). Momentum and Thermal Boundary-layer Thickness in a Stagnation Flow Chemical Vapor Deposition Reactor. *J. Materials Res.*, 12:1112–1121.

Dunlop, D. J. (1990). Developments in Rock Magnetism. *Rep. Prog. Phys.*, 53:707–792.

Dunlop, D. J., and Özdemir, Ö. (1997). *Rock Magnetism–Fundamentals and Frontiers*. Cambridge University Press, Cambridge.

Evans, M. E., and Heller, F. (2003). *Environmental Magnetism: Principles and Applications of Enviromagnetics: International Geophysics Series* (Volume 86). Academic Press, San Diego, CA.

Gao, P., Jaques, P. A., Hsiao, T. C., Shepherd, A., Eimer, B. C., Yang, M., et al. (2011). Evaluation of Nano- and Submicron Particle Penetration Through Ten Nonwoven Fabrics Using a Wind-Driven Approach. *J. Occup. Environ. Hyg.*, 8:13–22.

Hersh S. P., and Tucker, P. A. (1993). *Design and Evaluation of Improved Barrier Fabrics for Protection Against Toxic Aerosols and Biological Agents*. North Carolina State University College of Textiles for US Army Natick RD&E Center, Raleigh, NC. NATIC/TR-93/040.

Hunt, C. P., Moskowitz, B. M., and Banerjee, S. K. (1995). Magnetic Properties of Rocks and Minerals, in *Rock Physics & Phase Relations: A Handbook of Physical Constants*, Aherns, T. J., ed. American Geophysical Union, Washington, DC, pp. 189–204.

Jaques, P. A., Hopke, P. H., and Gao, P. (2012). Quantitative Analysis of Uniquely Distributed Submicron Paramagnetic Fe_3O_4 Particles Using Computer Controlled Scanning Electron Microscopy. *Aerosol Sci. Technol.*, 46(8):905–912.

Jaques, P. A., Hsiao, T. C., and Gao, P. (2011). A Recirculation Aerosol Wind Tunnel for Evaluating Aerosol Samplers and Measuring Particle Penetration Through Protective Clothing Materials. *Ann. Occup. Hyg.*, 55(7):784–796.

Kirchner, C., Liedl, T., Kudera, S., Pellegrino, T., Javier, M. U., Gaub, H. E., et al. (2005). Cytotoxicity of Colloidal CdSe and CdSe/ZnS Nanoparticles. *Nano. Lett.*, 5:331–338.

Lai, A. C. K. (2005). Modeling Indoor Coarse Particle Deposition onto Smooth and Rough Vertical Surfaces. *Atmos. Environ.*, 39:3823–3830.

Li, L., Greenberg, P. S., Street, K. W., and Chen, D. R. (2011). Study of a Magnetic Filter System for the Characterization of Particle Magnetic Property. *Aerosol Sci. Tech.*, 45:327–335.

Liu, B. Y. H., and Ahn, K. (1987). Particle Deposition on Semiconductor Wafers. *Aerosol Sci. Technol.*, 6:215–224.

Nazaroff, W. W., Ligocki, M. P., Ma, T., and Cass, G. R. (1990a). Particle Deposition in Museums: Comparison of Modeling and Measurement Results. *Aerosol Sci. Technol.*, 13:332–348.

Nazaroff, W. W., Salmon, L. G., and Cass, G. R. (1990b). Concentration and Fate of Airborne Particles in Museums. *Environ. Sci. Technol.*, 24:66–77.

Okuyama, K., Kousaka, Y., Yamamoto, S., and Hosokawa, T. (1986). Particle Loss of Aerosols with Diameters between 6 and 2000 nm in Stirred Tank. *J. Colloid Interface Sci.*, 110:214–223.

Scheneider, T., Bohgard, M., and Gudmundsson, A. (1994). A Semiempirical Model for Particle Deposition onto Facial Skin and Eyes. Role of Air Currents and Electric Fields. *J. Aeroso1 Sci.*, 25:583–593.

Slinn, W. G. N. (1982). Predictions for Particle Deposition to Vegetative Canopies. *Atmos Environ.*, 16:1785–1794.

Svoboda, J. (2004). *Magnetic Techniques for the Treatment of Materials*. Kluwer Academic, Dordrecht.

Turner, J. R., Liguras, D. K., and Fissan, H. J. (1989). Clean Room Applications of Particle Deposition from Stagnation Flow: Electrostatic Effects. *J. Aerosol Sci.*, 20:403–417.

Vinzents, P. S. (1996). A Personal Passive Dust Monitor. *Ann. Occup. Hyg.*, 40:261–280.

Wagner, J., and Leith, D. (2001). Passive Aerosol Sampler. Part I: Principle of Operation. *Aerosol Sci. Technol.*, 34:186–192.

Wood, N. B. (1981). The Mass Transfer of Particles and Acid Vapour to Cooled Surfaces. *J. Inst. Energy*, 76:76–93.

Yamamoto, N., Hikono, M., Koyama, H., Kumagai, K., Fujii, M., and Yanagisawa, Y. (2006). A Passive Sampler for Airborne Coarse Particles. *J. Aerosol Sci.*, 37:1442–1454.

Zhao, B., Chen, C., Yang, X., and Lai, A. C. K. (2010). Comparison of Three Approaches to Model Particle Penetration Coefficient Through a Single Straight Crack in a Building Envelope. *Aerosol Sci. Technol.*, 44:405–416.